



**HAL**  
open science

## **A water soluble probe with near infrared two-photon absorption and polarity-induced fluorescence for cerebral vascular imaging**

Julien Massin, Azzam Charaf-Eddin, Florence Appaix, Yann Bretonnière, Denis Jacquemin, Boudewijn van Der Sanden, Cyrille Monnereau, Chantal Andraud

### ► To cite this version:

Julien Massin, Azzam Charaf-Eddin, Florence Appaix, Yann Bretonnière, Denis Jacquemin, et al.. A water soluble probe with near infrared two-photon absorption and polarity-induced fluorescence for cerebral vascular imaging. *Chemical Science*, 2013, 4 (7), pp.2833-2843. 10.1039/c3sc22325f . inserm-00856213

**HAL Id: inserm-00856213**

**<https://inserm.hal.science/inserm-00856213v1>**

Submitted on 23 Apr 2014

**HAL** is a multi-disciplinary open access archive for the deposit and dissemination of scientific research documents, whether they are published or not. The documents may come from teaching and research institutions in France or abroad, or from public or private research centers.

L'archive ouverte pluridisciplinaire **HAL**, est destinée au dépôt et à la diffusion de documents scientifiques de niveau recherche, publiés ou non, émanant des établissements d'enseignement et de recherche français ou étrangers, des laboratoires publics ou privés.

Cite this: DOI: 10.1039/c0xx00000x

www.rsc.org/xxxxxx

ARTICLE TYPE

# A water soluble probe with near infra-red two-photon absorption and polarity-induced fluorescence for cerebral vascular imaging

Julien Massin,<sup>a</sup> Azzam Charaf-Eddin,<sup>b</sup> Florence Appaix,<sup>c</sup> Yann Bretonnière,<sup>a</sup> Denis Jacquemin,<sup>b,d\*</sup> Boudewijn van der Sanden,<sup>c\*</sup> Cyrille Monnereau<sup>a\*</sup> and Chantal Andraud<sup>a</sup>

<sup>5</sup> Received (in XXX, XXX) Xth XXXXXXXXXX 20XX, Accepted Xth XXXXXXXXXX 20XX

DOI: 10.1039/b000000x

A water soluble Lemke chromophore's derivative shows unusual polarity dependence of its emission efficiency, leading to a strong red-NIR fluorescence in water when fitted with appropriate water-solubilizing polymer chains. In this contribution, the synthesis of the chromophore is described. The  
10 dependence of its fluorescence on solvent polarity is investigated experimentally then rationalized on the basis of *ab initio* calculations. Finally, we demonstrate that this chromophore is a valuable candidate for *in vivo* two-photon imaging of the cerebral vasculature, with two-photon absorption and emissions in the biological transparency window.

## Introduction

<sup>15</sup> In recent years, two-photon laser scanning microscopy (TPLSM), especially intravital, has emerged as an essential tool in biomedical research and has nowadays become a routine technique to track biological processes down to the cellular level in the living animal.<sup>1-4</sup> In this context, fluorophores presenting  
20 electronic transitions of the "intramolecular charge transfer" (ICT) type are considered as a particularly appealing class of molecules. The peculiar linear (environmental sensitivity, solvatochromism<sup>5</sup>) and non-linear (two-photon absorption,<sup>6-8</sup> second harmonic generation<sup>9</sup>) spectroscopic properties associated  
25 to ICT transitions have been taken advantage of for the development of functional materials, including pH<sup>10,11</sup> or polarity probes<sup>12,13</sup> and biosensors<sup>14,15</sup> with one or two-photon induced fluorescence. These fluorophores are inherently lipophilic, because of their extended conjugated carbon backbone.<sup>6</sup> Thus,  
30 major efforts have been put on the improvement of their solubility in biological media and their biocompatibility. In that context, it has been shown by Müllen and coll. that controlled growth of a star-shaped polymer shell around a central fluorophore was a particularly effective strategy.<sup>16-18</sup> Moreover,  
35 we have recently given a proof of principle that such structures were valuable candidates for the vectorization of two-photon fluorophores into cells.<sup>19</sup> We showed that the resulting structures showed good-to-very-good conservation of their two-photon brightness in aqueous medium, with emission wavelengths up to  
40 570 nm. This result was however not fully optimal for *in-vivo* two-photon imaging applications, since it is desirable that the probe features maximal fluorescence in the biological window, *ie* at a wavelength between 700-1000 nm.<sup>20-22</sup>

<sup>45</sup> In this range of wavelengths, it is well documented that the fluorescence efficiency of strongly solvatochromic ICT chromophores is generally decreased. This can be explained on

the basis of the energy gap law, which postulates that non-radiative decay kinetic constants increase exponentially upon decreasing emission energy.<sup>23-25</sup> Moreover this energy gap  
50 mediated quantum yield (QY) decrease is often amplified in polar and/or protic solvents because of enhanced electrostatic interactions of the latter with the chromophore's strongly polarized ICT excited state.<sup>26</sup> Finally, as mentioned above, ICT chromophores are generally inherently hydrophobic, which can  
55 lead to formation of molecular aggregate in protic solvents such as alcohols or *a fortiori* water and can give rise to multiple additional non-radiative decay pathways.<sup>27</sup>

In a recent paper, several of us reported a series of red emitting Lemke's fluorophores (named after their initial discoverer<sup>28</sup>)  
60 based on an dicyanoisophorone motif, as solid state luminescent materials.<sup>29</sup> Beside their solid-state fluorescence, another spectroscopic property raised our interest: whereas these red fluorophores were hardly emitting in low-polarity solvents, like toluene, we noticed that their fluorescence QY gradually  
65 increased upon increasing solvent polarity. We felt that this particular feature could be taken advantage of in the context of bio-imaging applications which require probes that feature strong emission intensity in physiological fluids, preferentially in the biological transparency window.<sup>30,31</sup> We must underline that  
70 although Lemke's type chromophores have been extensively investigated in the context of second order nonlinear optics<sup>32</sup> (second harmonic generation<sup>33</sup> and electro-optic modulation<sup>34-36</sup>), their luminescence properties have surprisingly been only sparingly studied and mostly in the solid state, these compounds  
75 being considered essentially non emissive in solution.<sup>29,37,38</sup> Thus, in the present paper, we report the full study of the first example of a water soluble Lemke's chromophore oligomerised derivative (**Lem-PHEA**) and of its precursor (**Lem-In**). We show for the first time that both compounds display unusually strong

polarity induced enhancements of their luminescence QY along with significant red-shift of their emission, to reach, in the case of **Lem-PHEA**, 0.25 at 674 nm in water. Moreover, based on theoretical calculations we suggest a possible explanation regarding the origin of this peculiar behaviour, namely a solvent mediated change in the potential energy surface of the first electronically excited state of the molecule. This makes the latter a good candidate for *in vivo* two-photon imaging of the cerebral vascular in the biological transparency window.

## 10 Results and discussion

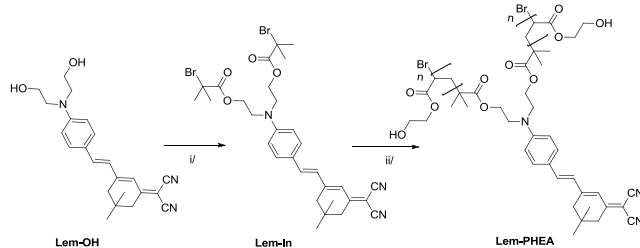
### Synthesis

Oligomerized compound **Lem-PHEA** was synthesized following the general methodology introduced in a previous paper<sup>19</sup> and depicted in Scheme 1. In a first step, a bromoisobutyryl moiety, which is classically used as a polymerization initiator in ATRP synthesis, was introduced through a simple, high yielding esterification procedure on the two terminal hydroxyl groups of **Lem-OH** precursor (which was itself obtained by well-established literature procedures). The resulting compound, **Lem-In**, was then involved in an ATRP polymerisation procedure with (hydroxyethyl)acrylate (HEA) used as a monomer, a Cu(II)/bipy catalyst, and THF as a co-solvent for the reaction. This procedure allowed to obtain an oligomerized object with precise control over chain length (*ca* 10-12 monomer unit on each arm, as calculated from <sup>1</sup>H NMR integrations) as evidenced by <sup>1</sup>H NMR and GPC (Figures S8). **Lem-PHEA** and its precursors **Lem-OH** and **Lem-In** were further characterized by <sup>1</sup>H and <sup>13</sup>C NMR (Figure S7), IR, UV-vis and fluorescence spectroscopy (see experimental for details).

### Linear spectroscopy: experiments

Spectroscopic measurements were next undertaken on the polymeric **Lem-PHEA** and its precursor **Lem-In**. As mentioned in introduction, solution luminescence spectroscopy of this class of chromophores had never been the object of systematic, detailed investigations in previous literature. Thus, this study was mainly aiming at elucidating some of the relation that exists between the solvent dependent emission energy of the fluorophore and other key spectroscopic parameters of the later (spectral bandwidth, Stokes shift...), in order to better understand the origin of its polarity induced emission.

To this end, **Lem-In** and **Lem-PHEA** were studied in different



**Scheme 1.** Synthetic pathway ; reagents and conditions: (i) 2-bromoisobutyryl bromide (3 eq.), Pyridine / THF 1:1, RT, 1h (ii) CuBr (1 eq.), bipyridine (2 eq.), 2-hydroxyethylacrylate (HEA) /THF (1 : 1), 85°C, 20 min

solvents that were chosen to cover the largest possible range of polarity, viscosities, and protic or non-protic character. Absorption and fluorescence emission spectra of both compounds were systematically recorded. Quantum yields (QY) were calculated from integration of the fluorescence intensity at various concentrations and comparison to a standard (erythrosine). Absorption and emission curves are reported in Figure 1 whereas the main spectroscopic values are listed in Table 1.

First of all, for both compounds, broad, structureless emission bands were observed in all solvents of the study, which confirms the ICT character of the emission. The tendency observed qualitatively in our previous report (see Introduction) was fully verified for both objects: upon increasing solvent's polarity (according to Lippert's polarity scale) from toluene to DMSO for **Lem-In** and from dioxane to water for **Lem-PHEA**, a significant red-shift of the emission energy was observed (positive solvatochromism), which was accompanied with a marked increase of fluorescence QY (negative solvatochromism) along with progressive narrowing of the emission band. A plot of the

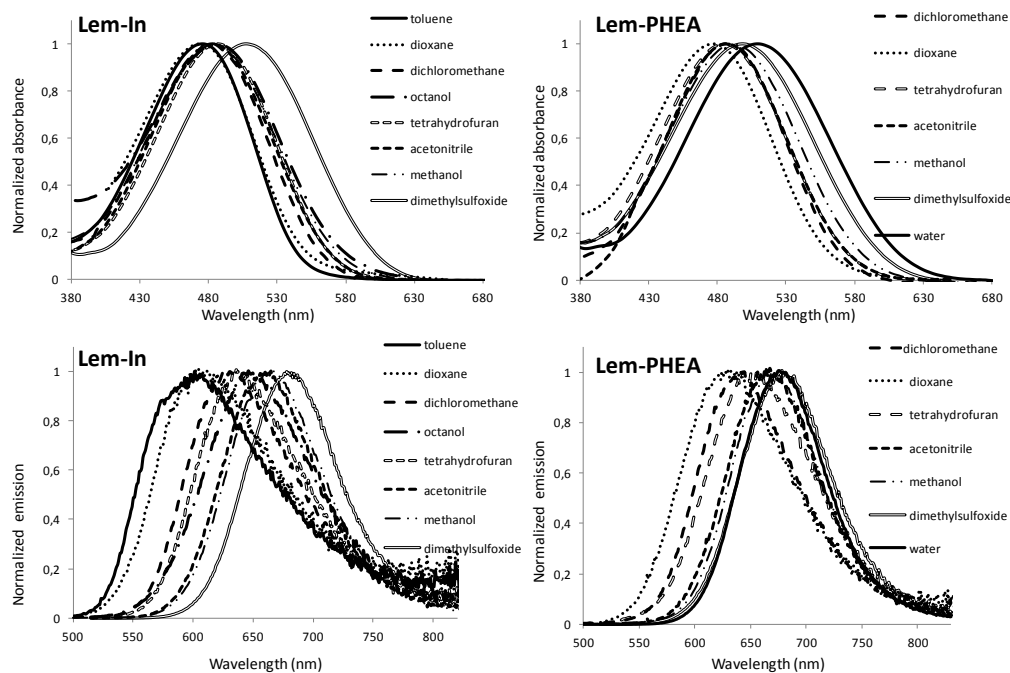


**Figure 1.** Normalized absorption (top) and emission (bottom) spectra of Lem-In (left column) and Lem-PHEA (right column) in the solvents of the study

Table 1. Relevant spectroscopic data

	Solvent	$\Delta f$	$\lambda_{\text{max}}$ (nm)	$\lambda_{\text{em}}$ (nm)	$\Delta \bar{\nu}$ ( $\text{cm}^{-1}$ )	$\Delta \nu_{1/2}$ ( $\text{cm}^{-1}$ )	$\phi_f^a$	$\tau_f$ (ns) <sup>b</sup>	$\epsilon$ ( $\text{M}^{-1}\cdot\text{cm}^{-1}$ )	$\sigma_{\text{TPA}}$ (GM)
<b>Lem-In</b>	toluene	0.013	474	602	4490	3300	0.008	<0.1	27900	-
	dioxane	0.02	474	606	4600	3080	0.016	0.13	-	-
	$\text{CH}_2\text{Cl}_2$	0.21	482	630	4870	2550	0.025	0.2	28200	530
	$\text{CHCl}_3$	0.14	482	633	4950	2520	0.016	0.24	-	-
	TFH	0.21	486	637	4877	2440	0.04	0.3	-	-
	octanol	0.22	485	646	5140	2412	0.045	0.66	-	-
	AcCN	0.305	484	661	5530	2050	0.07	0.5	-	-
	MeOH	0.31	484	664	5600	2045	0.1	0.7	-	-
DMSO	0.26	508	680	4979	1940	0.3	1.3	30200	-	
<b>Lem-PHEA</b>	dioxane	0.02	478	630	5050	2920	0.049	0.48	-	-
	$\text{CH}_2\text{Cl}_2$	0.21	490	640	4780	2400	0.045	0.58	-	-
	$\text{CHCl}_3$	0.14	494	642	4670	2680	0.032	0.53	-	-
	TFH	0.21	486	652	5240	2562	0.083	0.65	-	-
	AcCN	0.305	483	668	5730	2080	0.12	0.67	-	-
	MeOH	0.31	494	670	5317	1980	0.14	0.86	-	-
	DMSO	0.26	500	678	5250	2050	0.26	1.34	-	-
	$\text{H}_2\text{O}$	0.32	510	676	4810	1930	0.22	1.14	21000	440

a/  $\lambda_{\text{ex}} = 488$  nm, reference is erythrosine in MeOH ( $\phi_{\text{ref}}=0.09$ ), error margin  $\pm 5\%$  b/  $\lambda_{\text{ex}} = 490$  nm, error margin  $\pm 5\%$

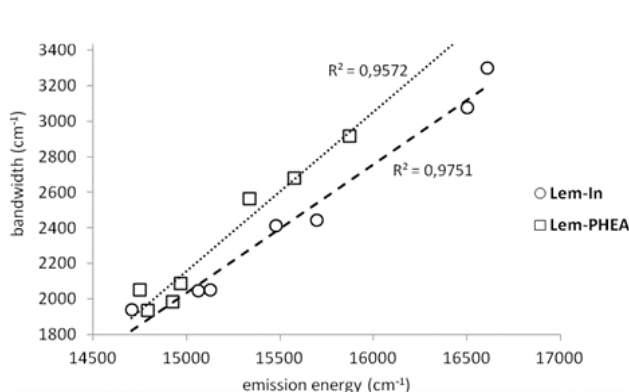


**Figure 2.** Plot of emission band-width vs energy at the maximum of the emission (as found in the solvatochromic study, Table 1). Linearization were performed independently for data obtained with **Lem-In** (dashed line) and **Lem-PHEA** (dotted line)

emission bandwidth *versus* emission energy clearly reveals, for **Lem-In** and **Lem-PHEA**, a close to linear dependence between those two parameters, with a bandwidth that narrows upon decreasing emission energy (Figure 2). Meanwhile, the band shape becomes more symmetric as the emission energy decreases and a Gaussian shape is observed in most polar solvents (e.g. water and DMSO). Interestingly, this tendency is absolutely similar for **Lem-PHEA** and its precursor **Lem-In**. Such an evolution, which will be further commented in the following, is opposed to what is classically observed for ICT fluorophores exhibiting positive solvatochromism: their emission band generally tends to become more broadened and structureless as solvent polarity increases, as a consequence of increased interactions with the solvent.<sup>5</sup>

Changes in emission energy and dependence of the Stokes shifts values on solvent polarity are important features in the context of ICT chromophores, since both parameters can be used in the engineering of polarity probes.<sup>5, 39</sup> On a more fundamental point of view, their study allows determining some important

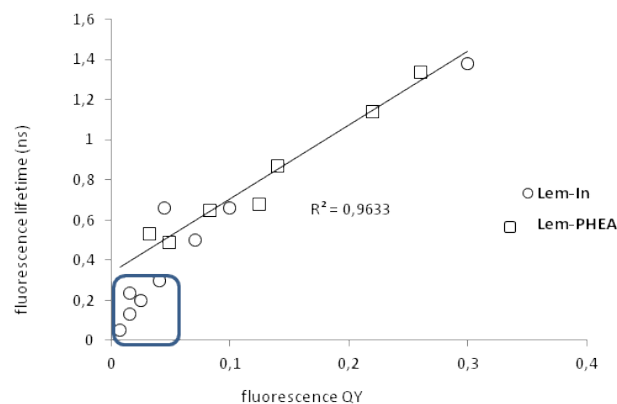


**Figure 3.** Plot of fluorescence quantum yield vs excited state lifetime ((as found in the solvatochromic study, Table 1); data in the blue frame correspond to fluorescence lifetime  $\leq 0.3$  ns, which corresponds to the lower limit of the detector, hence cannot be considered meaningful. Linear regression was performed on the joint data for **Lem-In** and **Lem-PHEA**

parameters of the molecule, like its dipolar moment at the ground ( $\mu_g$ ) and excited ( $\mu_e$ ) states and the electronic reorganisation (change in dipole moment  $\mu_{\text{CT}}$ ) that accompanies the transition between the ground and excited states.<sup>40, 41</sup> These parameters were thus investigated for **Lem-In** and **Lem-PHEA**. In the case of **Lem-In**, absorption and emission energies as well as Stokes shift values showed a clear tendency to increase upon increasing solvent polarity (positive solvatochromism), thereby indicating an increased dipole moment at the excited state. This is consistent with what had been observed for related chromophores in our previous contribution.<sup>29</sup> The trend could be fitted with an acceptable correlation factor to Lippert-Mataga polarity scale<sup>13, 42, 43</sup> (Figure S1) which allowed us to estimate dipole moments of the chromophore at its ground and excited states of  $\mu_g = 10.5$  D and  $\mu_e = 24.5$  D, respectively, and a change in dipole moment  $\mu_{\text{CT}} = 13.5$  D. The situation is however not so straightforward to analyze for **Lem-PHEA**, since the polarity environment of the chromophore is in this case not only determined by the nature of

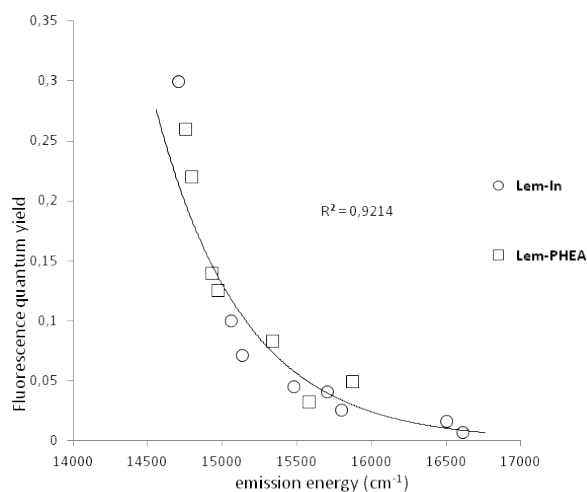


**Figure 4.** Plot of fluorescence quantum yield vs emission energy (as found in the solvatochromic study, Table 1). Exponential fit was performed on the joint data for **Lem-In** and **Lem-PHEA**

the solvent, but by a more subtle interplay between chromophore/solvent and chromophore/polymer chain interactions. Indeed, it had been already established in our previous contribution devoted to alike water-soluble polymerized chromophores<sup>19</sup> that the polymer chain adopts different folding and orientations around the chromophore depending on the nature of the solvent. Thus, we were unable to identify a clear trend in Stokes shift and emission band position for **Lem-PHEA** (Figure S1).

Excited state lifetimes were also investigated for both systems in the same range of solvents as for QY measurements. A near-linear dependence of fluorescence quantum yield on excited state lifetime could be noticed. The trend was so alike for both compounds that their data were fitted jointly (Figure 3). These data allowed us to calculate radiative ( $k_r$ ) and non-radiative ( $k_{nr}$ ) kinetic constants for excited state decay (Figure S3): although  $k_r$  slightly increases with solvent polarity, it remains in a comparable range in every solvent ( $0.8 - 1.9 \times 10^8 \text{ s}^{-1}$ ). In striking contrast, it can be noticed that a variation of more than one order of magnitude is observed for  $k_{nr}$  ( $1 \times 10^{10}$  to  $7 \times 10^8 \text{ s}^{-1}$ ). Altogether, this constitutes an unambiguous evidence that variations of the fluorescence quantum efficiency are mainly connected to modifications in the non-radiative excited state decay kinetic which decreases as polarity increases.

An even more peculiar spectroscopic behaviour of these fluorophores was detected when plotting the evolution of their luminescence quantum efficiency (Figure 4) or alternatively effective. In Table S-1 in SI, we compare the XRD and DFT bond lengths fluorescence lifetime (see Figure S2) versus emission energy. Whereas the energy gap law predicts an exponential increase of non-radiative excited state decay kinetics and therefore an exponential decrease of the quantum efficiency upon red-shift of the luminescence,<sup>24</sup> the observed evolution for our dyes seems to follow a fully reverse trend. Indeed, the data obtained for both **Lem-In** and **Lem-PHEA** could be jointly fitted with satisfactory accuracy ( $r^2 = 0.921$ ) to an inverse model, with an exponential increase of fluorescence lifetime and quantum efficiency upon luminescence red-shift. As mentioned before, this

evolution is correlated with a significant sharpening of the emission band. This is indicative that the vibronic contributions or the nature of the potential energy surfaces which result in the shoulder of the emission band in low-polarity solvents (see toluene), tend to vanish in polar ones (see DMSO). These changes also translate into the increased non-radiative contribution to the ES decay observed in non-polar solvents (Figure S3). This point will be further discussed in the next section of this article. As a result, **Lem-In** and **Lem-PHEA** show a strongly negative solvatokinetic, *ie* their largest luminescence intensity was obtained in the most polar solvents of the study (DMSO for **Lem-In**, DMSO and water for **Lem-PHEA**). A closer examination of the data rules out simple explanations that could account for this peculiar behaviour, such as restriction of vibronic deactivations of the excited state through hydrogen bonding or solvent viscosity. On the one hand, hydrogen-bond donor solvents, such as octanol, methanol and water perfectly follow the overall trend, and do not show any remarkable behaviour. On the other hand, solvents of close polarity, but of very different viscosities such as THF (*ca*  $\eta = 0.5 \text{ cP}$ ) and octanol (*ca*  $\eta = 9 \text{ cP}$ ) show similar results in terms of fluorescence efficiency of the probes. An interesting consequence for biophotonic related applications is that, in contrast to most existing fluorescent bio-probes and polarity sensors, **Lem-PHEA** presents a luminescence that is turned on in a polar environment like blood or physiological fluid. This can be a very favourable feature for angiographic applications as we will discuss latter.

#### Linear spectroscopy : theoretical calculations

To obtain further insights regarding the nature of the excited-states, and to assess the origin of the experimentally observed polarity induced fluorescence Time-Dependent Density Functional Theory (TD-DFT) calculations have been performed on a model compound, referred to as **Lem** (Figure 5a, see Experimental Section for computational details). First, calculations were carried out with the least polar solvent, namely toluene, for which the selected continuum solvation model, which does not account for any specific solute-solvent interaction(s),

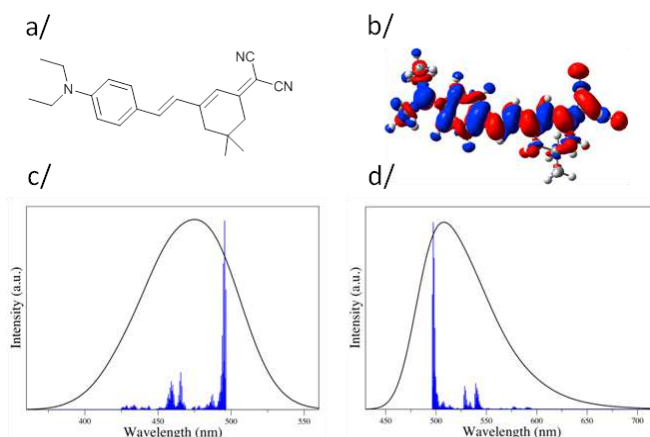


**Figure 5:** Left (a) Model compound (**Lem**) used for calculations (b) density difference plot computed in toluene: red (blue) zones correspond to increase (decrease) of density upon photon absorption (isovalue:  $6 \times 10^{-4} \text{ a.u.}$ ) (c) stick and convoluted vibrational absorption spectra in toluene. (d) stick and convoluted vibrational emission spectra in toluene.

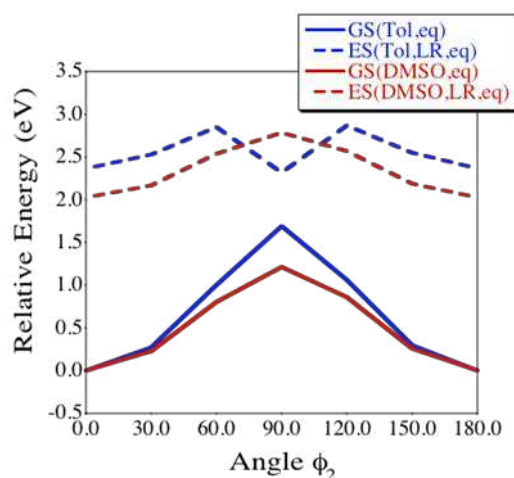


**Figure 6:** Evolution of the relative energies of the GS and ES of Lem in toluene and DMSO, for twist around  $\phi_2$ .

should be very measured along the  $\pi$ -conjugated path. As can be seen, there is a very good agreement between theory and experiment for both absolute distances ( $MAD < 0.01 \text{ \AA}$ ) as well as the bond length alternation (BLA), which confirms the accuracy of the selected level of theory. Moving from the ground to the lowest-lying excited state (which is the only state accessible in this range of energy, as confirmed by our calculations) induces a strong decrease of the BLA ( $-0.033 \text{ \AA}$ ), which is characteristic of a more delocalized excited-state, as expected. In the same vein, the density-difference plot (Figure 5b) clearly confirms a strong CT character from the diethylamino side to the cyano groups, with a significant electronic reorganization on the connecting bridge. The ICT distance, estimated as the separation between the barycenters of electron density gain/loss, reaches  $3.75 \text{ \AA}$  and is accompanied by a strong enlargement of the dipole moment ( $+11.8 \text{ D}$ ) upon electronic transition, a trend that is in remarkable agreement with the experiment (see above). The vibrationally resolved absorption and emission spectra can be found in Figures 5c and 5d, respectively. For absorption, one computes a maximum at  $453 \text{ nm}$ , which is close to the experimental spot ( $474 \text{ nm}$ ). The theoretical FWHM is  $3610 \text{ cm}^{-1}$  for the absorption band. Apart from low-frequency vibrations close to the 0-0 point, the width of the absorption band can be explained by a series of vibronic couplings in the  $430\text{--}445 \text{ nm}$  domain. They imply to a complex mix of modes, but the strongest contributions correspond to intense stretching modes related to the alteration of the single/double bond nature along the conjugated skeleton. For instance, an effective conjugation coordinate (ECC) mode at  $1607 \text{ cm}^{-1}$  (in the ES) located on the central vinylic moiety is responsible for the most intense peak close to  $430 \text{ nm}$ . Consistently with measurements, the fluorescence band is also asymmetric, and presents a FWHM of  $2859 \text{ cm}^{-1}$ , which is slightly above the experimental reference ( $3300 \text{ cm}^{-1}$ , see Table 1). However, the computed position of  $\lambda_{em}$  is  $482 \text{ nm}$ , significantly off the experiment ( $602 \text{ nm}$ ): the TD-DFT Stokes shift is clearly too small. In short, despite an undershot Stokes shift, theory reproduces nicely the band shapes in toluene. We have also simulated the same data in DMSO (Figure S6). In

DMSO, the BLA is slightly smaller to the one computed in the apolar environment for the ground-state ( $0.056 \text{ \AA}$  in DMSO versus  $0.061 \text{ \AA}$  in toluene), the reverse holding for the excited-state ( $0.034 \text{ \AA}$  in DMSO versus  $0.028 \text{ \AA}$  in toluene). Therefore the GS/ES variation of the main geometrical parameters related to optical properties is smaller in DMSO than in toluene. However, the increase of dipole moment upon absorption ( $+13.5 \text{ D}$ ) significantly exceeds the toluene value. Moreover, we computed a FWHM of  $3094 \text{ cm}^{-1}$  for the fluorescence in DMSO, which is almost unchanged from toluene. This clearly departs from experimental trends ( $1800 \text{ cm}^{-1}$ ). Likewise, the fluorescence band is slightly asymmetric in the calculations (Figure S6), which also contrasts with the measurements. To estimate the importance of the non-radiative path, we determined the Huang-Rhys (HR) factors, following the procedure of Peng *et al.*<sup>44</sup> We found that the HR factor decreases from toluene to DMSO. This indicates that non-radiative paths are less effective in the latter and therefore that fluorescence efficiency should increase. Although this result is in qualitative agreement with our experimental observations, the calculated effect ( $-5\%$ ) appears significantly too small to fully account for the dramatic experimental variation, which led us to envision other hypotheses. The theory/experiment differences might be ascribed to i) aggregation, ii) specific solute-solvent interactions iii) anharmonicity or iv) change in the nature of the potential energy surface that are not included in the previous model. The two first factors can be reasonably excluded: on the one hand, aggregation can be almost fully discarded on the basis of concentration-dependence studies on the absorption and fluorescence spectra; on the other hand, simple hydrogen-bonding can be ruled out on the basis of our experiments (*vide supra*). Interestingly, the third factor (anharmonicity) is known to induce significant deviation from the standard energy-gap law, which could potentially account for the experimentally observed trend for the fluorescence QY.<sup>45</sup> Rotation of the terminal groups at the ES could also account for the experimental trends (fourth factor). Interestingly, investigations on this parameter revealed significant qualitative differences between toluene and DMSO (Figures S4-S5, Figure 6). Indeed, while rotation around the dimethylamino moiety does not yield new minima on both GS and ES surfaces, the rotation around the dicyanovinylene group (angle  $\phi_2$ , Figure S4) yields a twisted minimum ( $90^\circ$ ) of the ES in toluene, that is absent from the ES in DMSO (Figure 6). Consequently, the ES of

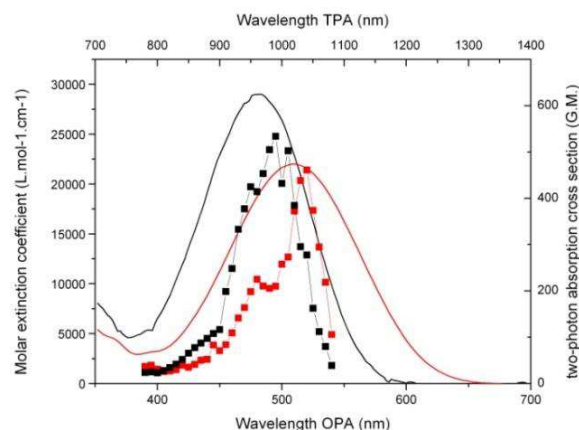


**Figure 7.** One- (full) and two-photon (full with marks) absorption spectra of Lem-In in dichloromethane (black) and Lem-PHEA in water (red)

the emitter is predicted to be more rigid in DMSO than in toluene, which in turn could account for the difference of band shapes. As can be seen in Figure 6, this 90° structure presents an energetic minimum at the ES, slightly lower in energy than the planar conformation. Interestingly GS and ES energies of this 90° structure are very close on the energetical scale, hinting a possible conical intersection<sup>46</sup> that would offer a supplementary non-radiative pathway in toluene but not in DMSO. To say it differently, we suggest that the much lower ES-GS energy gap of the 90° twisted structure could explain its non-emissive nature. This leads us to conclude that the very strong reverse solvatokinetic effect observed experimentally cannot be fully explained by harmonic vibronic couplings, or by electrostatic effects between the solute and the solvent, but is most likely related to a change of the surface potential at the ES.

## Two-photon absorption

Two-photon absorption properties of **Lem-PHEA** in water were evaluated and compared with those of its precursor **Lem-In** in dichloromethane, in order to determine whether our strategy also allowed an adequate conservation of this parameter. Two-photon absorption cross-sections ( $\sigma_{\text{TPA}}$ ) were measured using two-photon induced fluorescence experiments (see material and methods section for details). The results are reported in figure 7, along with the linear absorption spectra **Lem-In** and **Lem-PHEA** in corresponding solvents. From these experiments, it is clear that only a slight decrease of  $\sigma_{\text{TPA}}$  occurs between **Lem-In** in dichloromethane and **Lem-PHEA** in water, which is found to reflect the evolution their respective linear molar extinction coefficient. This demonstrates that **Lem-PHEA**, with a  $\sigma_{\text{TPA}} = 440 \text{ GM}$  and a maximal two photon brightness ( $\sigma_{\text{TPA}} \cdot \phi_f$ ) of about 100 GM, is unarguably a valuable candidate for the target application.

## In vivo two-photon microscopy

In order to evaluate its potential as bio-marker, **Lem-PHEA** was used in TPLSM of the functional cerebral vasculature in the motor cortex of mice brain, see materials and methods section. As it could be anticipated from the emission spectrum of the probe in water, its fluorescence emission intensity *in vivo* was higher in the NIR region in comparison to the red region (Figure S9) for an excitation wavelength of 950 nm. At this excitation wavelength no background endo-fluorescence of tissues was detected. After intra-venous (i.v.) injection, **Lem-PHEA** circulated freely in the blood plasma with no adhesion to the vessel wall (Figure 8a), This is important for, i) longitudinal imaging of the blood circulation, and ii) decreased long-term vascular toxicity. The red/NIR fluorescent emission *in vivo* is less diffused by brain

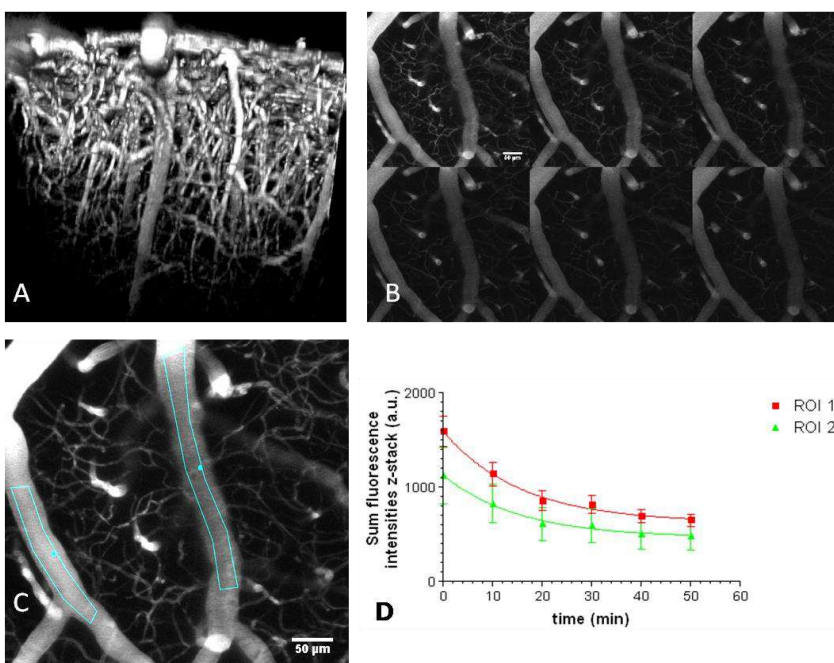


**Figure 8** Functional cerebral vasculature in motor cortex of a 6 months old CD1 mouse at different times after i.v. injection of Lem-PHEA. 7a) Lateral view of the 3D-reconstruction of a z-stack until a depth of 520  $\mu\text{m}$  at 5 min after i.v. injection of Lem-PHEA showing the plunging arteries and draining veins. 7b) Z-projections of the sum of fluorescence intensities at 10,20,30,40 50 and 60 min after injection. 7c) A Z-projection of the sum of the intensities at 10 min showing the ROI 1 & 2 for half-life time analysis. 7d) Half-time analysis of Lem-PHEA in the blood plasma using a one phase mono-exponential decay ( $Y = \text{Span} \cdot \exp(-K \cdot x)$ ), the values are the means of fluorescence intensities in the ROI (z-projection of the sum of the intensities) with their standard deviations (bars): results curve fitting (GraphPad Prism version 3.02, GraphPad Software, Inc, La Jolla, CA, USA): ROI 1=  $K = 0.06429$ , half-life time = 10.78 min,  $R^2 = 0.993$ , Fit data ROI 2 =  $K = 0.06472$ , half-life time = 10.71 min,  $R^2 = 0.990$ . Scale bar = 50  $\mu\text{m}$ .

tissues, which resulted in a maximal observation depth of 520  $\mu\text{m}$  in the adult mouse brain (Figure 8a) at normal laser power for *in vivo* experiments: maximum 50 mW at the entrance of the objective.

In a time series experiment, the half-life time of **Lem-PHEA** in the blood plasma was estimated in the order of 11 min (see Figure 8b-d). The clearance of the dye by the kidneys started already at 30 min after injection (Figure S10a). At this time the dye is observed in collecting tubules of the kidney and after two hours no dye was detected in the renal vascular compartment (Figure S10b-c). In the liver, **Lem-PHEA** stayed in the vascular compartment and was not found in hepatic cells for at least 2 hours after injection (Figure S10d). Thus renal clearance of **Lem-PHEA** is most probably preferred over liver metabolism of the dye. Such a fast renal clearance precludes its use for intravital microscopy studies of blood physiological phenomena exceeding 1 hour. On the other hand, it constitutes a very positive result with regard to long-term toxicity of the compound *in vivo*. In the future, it could be envisioned to extend **Lem-PHEA** circulation time by enhancing polymer chains length, as already illustrated in the past for related systems.<sup>47</sup>

## Experimental

### Materials and methods

#### Synthesis

All solvents were used as received from the supplier. 2-bromoisobutyryl bromide and bipyridine are commercially available and used as received from the suppliers. Copper (I) bromide (Aldrich, 98%) was suspended in glacial acetic acid, filtered and washed with acetic acid then thoroughly rinsed with ethanol. After extensive drying under vacuum it was stored at 4°C under argon. Hydroxyethylacrylate (HEA) was passed through a short pad of alumina prior to use. (*E*)-2,2'-(4-(2-(3-Dicyanomethylene)-5,5-dimethylcyclohex-1-enyl)(vinyl)phenylazanediy)bis(ethane)bis(ethane-2,1-diyl)diacetate was synthesized according to previously reported literature methodologies.<sup>29</sup> Column Chromatographies were performed on Merck Gerduran 60 (40-63 μm). NMR spectra (<sup>1</sup>H, <sup>13</sup>C) of the monomers and polymers were recorded at room temperature on a BRUKER 200 AVANCE and BRUKER 500 respectively. Data are listed in parts per million (ppm) and are reported relative to tetramethylsilane (<sup>1</sup>H, <sup>13</sup>C), residual solvent peaks being used as internal standard. FTIR spectra (ATR) were performed on solid samples using a JASCO FT/IR 4100 spectrometer equipped with a JASCO ATR PRO450-S ATR module. HRMS measurements were performed by ESI-TOF: a Bruker Daltonics ® Micro TOF-Q II was used with a resolution of 8000, in positive mode with a capillary tension of 4500V, a source temperature of 180°C, and a cone tension of 60V. The internal reference used for calibration was sodium formate. Elemental analyses were performed on a Flash EA1112 CHNS/O Thermo Electron micro-analyzer. Polymers were analyzed by size exclusion chromatography (SEC) in DMF (+ LiBr, 1 g·L<sup>-1</sup>) at 60 °C, at a flow rate of 0.8 mL·min<sup>-1</sup> and at a concentration close to 6 mg·mL<sup>-1</sup> after filtration through 0.2 μm pore size membrane. The steric exclusion was carried out on two PSS GRAM 1000 Å columns (8 × 300 mm; separation limits: 1 to 1000 kg·mol<sup>-1</sup>) and one PSS GRAM 30 Å (8 × 300 mm; separation limits: 0.1 to 10 kg·mol<sup>-1</sup>) coupled with a differential refractive index (RI) detector, a viscosimeter (Viscotek, Dual 250) and a light scattering (LS) detector (MiniDawn from Wyatt Technology, laser λ = 690 nm at 90°, 45° and 135°). The polydispersity indexes (PDI = *M<sub>w</sub>*/*M<sub>n</sub>*) of the samples were derived from the RI signal by a calibration curve based on PMMA standards (Polymer Standards Service). The number-average molar mass (*M<sub>n</sub>*) were calculated from RI signals with the OmniSEC 4.6 software. Polymer size (*M<sub>n</sub>*) was also calculated with <sup>1</sup>H spectroscopy, by comparison of the integration values found for the methyl end-groups of the initiator (signal “a” of the polymer, SI), and for the side chain hydroxyethyl group (signals “d” and “e” of the polymer, SI).

### Spectroscopy

UV-Visible spectra were recorded with a Jasco 670 UV-Visible spectrophotometer. The luminescence spectra were measured using a Horiba-Jobin Yvon Fluorolog-3® spectrofluorimeter. The steady-state luminescence was excited by the unpolarised light from a 450W xenon CW lamp and detected at an angle of 90° for diluted solution measurements (10 mm quartz cuvette) by a red-sensitive Hamamatsu R928 photomultiplier tube. Spectra were reference corrected for both the excitation source light intensity variation (lamp and grating) and the emission spectral response (detector and grating). Fluorescence quantum yields *Q* were measured in diluted water solutions with an optical density lower

than 0.1 using the relative method based on following equation:

$$Q_x/Q_r = [A_r(\lambda)/A_x(\lambda)][n_x^2/n_r^2][D_x/Dr]$$

where *A* is the absorbance at the excitation wavelength (λ), *n* the refractive index and *D* the integrated luminescence intensity. “*r*” and “*x*” stand for reference and sample. Here, reference is erythrosine in MeOH (*Q<sub>r</sub>* = 0.45) at 488 nm. Excitation of reference and sample compounds was performed at the same wavelength. The TPA cross-section spectra were obtained by two-photon excited fluorescence measurement of dilute dichloromethane solutions of the compound using a Ti:sapphire femtosecond laser in the range 700-900 nm. The excitation beam (5 mm diameter) was focalized with a lens (focal length 10 cm) at the middle of the fluorescence cell (10 mm). The fluorescence, collected at 90° to the excitation beam, was focused into an optical fiber (diameter 600 μm) connected to an Ocean Optics S2000 spectrometer. The incident beam intensity was adjusted to 50 mW in order to ensure an intensity-squared dependence of the fluorescence over the whole spectral range. The detector integration time was fixed to 1 s. Calibration of the spectra was performed by comparison with the published 700-900 nm Coumarin-307 and fluorescein two photon absorption spectra.<sup>48</sup> The measurements were done at room temperature in dichloromethane and at a concentration of 10<sup>-4</sup> or 10<sup>-5</sup> M.

### Calculations

TD-DFT was used to probe the nature of the excited-states of the Lem dyes where the only structural simplification was the use of NEt<sub>2</sub> donating group (see Figure 6). We have applied a computational protocol similar to the one applied in a recent benchmark paper<sup>49</sup> and we redirect the interested reader to this contribution for further technical details and discussion. The ground and excited-state structures have been optimized using analytic DFT and TD-DFT gradients, respectively. These force minimizations have been performed until the residual mean square force is smaller than 1x10<sup>-5</sup> a.u. The harmonic vibrational frequencies of both states have been computed on the optimal geometries using analytic and numerical differentiation for GS and ES, respectively. This allowed to ascertain the nature of the minima but also to determine vibronic couplings. The vibrationally resolved spectra -within the harmonic approximation- were computed using the FCclasses program<sup>50, 51</sup>. The reported spectra have been simulated at 298K using a convoluting Gaussian functions presenting a full width at half-maximum (fwhm) of 0.06 eV. A maximal number of 25 overtones for each mode and 20 combination bands on each pair of modes were included in the calculation. The maximum number of integrals to be computed for each class was set to 1x10<sup>6</sup>. In our calculations, the electrostatic interactions between the dye and the environment have been modelled thanks to the PCM model that restores valid solvent effect, as long as no specific solute-solvent interactions take place.<sup>52</sup> The adiabatic energies and consequently the position of both absorption and fluorescence maxima in vibrationally resolved spectra have been evaluated using the state-specific (SS) PCM model that allows to correctly polarize the excited-state cavity.<sup>53</sup> Again, we redirect the interested reader to Ref. <sup>49</sup> for a detailed discussion on the procedure used to determine the adiabatic point. All our calculations have been performed with the Gaussian 09.A02 program<sup>54</sup> using the CAM-B3LYP functional<sup>55</sup> and the 6-31+G(d) atomic basis set that are



known to be a valuable combination for TD-DFT calculations.<sup>49</sup> The ICT parameters have been computed using a recently proposed density-based model.<sup>56</sup>

### 5 *In-vivo* two-photon microscopy

In accordance with the policy of Grenoble Institute of Neuroscience (GIN) and the French legislation, experiments were done in compliance with the European Community Council Directive of November 24, 1986 (86/609/EEC). The research involving animals was authorized by the Direction Départementale des Services Vétérinaires de l'Isère – Ministère de l'Agriculture et de la Pêche, France and the Direction Départementale de la protection des populations - Préfecture de l'Isère-France (F. Appaix, PhD, permit number 38 09 39). All efforts were made to minimize the number of mice used and their suffering during the experimental procedure. CD1 Mice were housed in cages with food and water *ad libitum* in a 12 h light/dark cycle at  $22 \pm 1$  °C.

For *in vivo* TPLSM, 6 months old CD1 mice (n=4) were anesthetized using isoflurane (5% for induction and 1-2% during experiments) in a 70% air, 30% O<sub>2</sub> gas mixture. Their body temperature was monitored with a rectal probe and maintained at 36°C using a heating blanket. A catheter (Neoflon™, BD, USA) was inserted in the tail vein for an intravenous (iv) injection of 0.1 ml Lem-PHEA solution at a concentration of 4 mg/ml just before the imaging experiments. For the two-photon imaging of the cerebral vasculature, a craniotomy of 2-3 mm in diameter was performed with a surgical drill above the motor cortex and filled with ultrasound gel. (The head was fixed in a homebuilt stereotactic frame.)

Two-photon microscopy was performed using a LSM 7 MP (Zeiss, Germany) equipped with a 20x water-immersion objective (NA 1.0; Zeiss) and ZEN 2010 software. Laser excitation at 950 nm was done with a Ti:Sapphire laser system (Chameleon Ultra II; Coherent, UK). Red Fluorescence light emission was collected in the epifluorescence configuration using a non-descanned photomultiplier tube with a 617/73 nm filter (Semrock, US). Most two-photon images were acquired as z-stacks with a maximum number of 257 images using the motorized objective with a minimal step of 2 μm between the different x-y planes (512 x 512 pixels, 607.28 μm<sup>2</sup>) resulting in a maximum observation depth of 520 μm in the motor cortex of an adult mouse. The reconstruction of z-projections: sum of fluorescence intensities of all focal planes in a z-stack, or generation of 3D images were performed with ImageJ software<sup>57</sup>.

### Syntheses

#### Lem-OH

(*E*)-2,2'-(4-(2-(3-Dicyanomethylene)-5,5-dimethylcyclohex-1-enyl)-(vinyl)phenylazanediy)l)-bis(ethane)bis(ethane-2,1-diy)diacetate (18 mmol) was dissolved in about 20 mL of methanol. Then, a solution of K<sub>2</sub>CO<sub>3</sub> (0.5g) dissolved in H<sub>2</sub>O (1 mL) was added and the mixture was stirred at room temperature. After 1 hour, the suspension was diluted with water (100 mL). The aqueous layer was extracted three times with CH<sub>2</sub>Cl<sub>2</sub> (3x50 mL) and the combined organic phases were washed with brine (50mL), dried over MgSO<sub>4</sub>, concentrated under reduced pressure and purified by flash column chromatography (ethyl acetate/pentane : 1/9) to obtain a pure dark reddish solid. Yield: 5.91 g (87 %).

<sup>1</sup>H NMR (d<sub>6</sub>-DMSO): δ(ppm) 7.37(d, *J*=9 Hz, 2H), 6.97 (m, 2H), 6.53 (m, 3H), 4.61(b, 2H), 3.33(m, 8H), 2.35(m, 4H), 0.81(s, 6H). <sup>13</sup>C NMR (d<sub>6</sub>-DMSO): δ(ppm)170.3, 158.0, 150.2, 139.2, 130.5, 124.2, 123.5, 120.5, 115.1, 114.3, 112.1, 58.6, 53.6, 42.8, 38.9, 32.1, 28.0. Anal.Calcd for C<sub>23</sub>H<sub>27</sub>N<sub>3</sub>O<sub>2</sub>+H<sub>2</sub>O: C, 69.85; H, 7.39; N, 10.62. Found: C, 69.51; H, 6.83; N, 10.43. HRSMS (ES): [M+ Na]<sup>+</sup> 400.1988 (calcd 400.1995)

#### Lem-In

**Lem-OH** (200mg, 0.53mmol) was dissolved in 5mL of THF and 130μL of pyridine (1.65mmol). To the resulting reddish solution were added dropwise 270 μL of bromoisobutryl bromide (500mg, 2.2 mmol), and the solution was stirred at room temperature for 1 hour. Then dichloromethane (10mL) was added, and the solution was extracted with 20 mL of 0,1M HCl. The organic layer was dried, and solvents were removed under reduced pressure. The residue (single spot on TLC) was purified by column chromatography on silica gel (CH<sub>2</sub>Cl<sub>2</sub>), and a reddish solid was obtained (190 mg, 56%)

<sup>1</sup>H NMR(CDCl<sub>3</sub>): δ(ppm) 7.42 (d, *J*=7.5 Hz, 2H), 7.00 (d, *J*=16Hz, 1H), 6.78 (m, 4H), 4.32(t, *J*=6Hz, 4H), 3.75 (t, *J*=6Hz, 4H), 2.52 (s, 2H), 2.42 (s, 2H), 1.87 (s, 12H), 1.04 (s, 6H). <sup>13</sup>C NMR (CDCl<sub>3</sub>): δ(ppm)171.3, 169.2, 155.0, 148.5, 137.5, 129.6, 125.1, 124.7, 121.8, 114.0, 113.2, 112.3, 62.9, 55.4, 49.1, 42.9, 39.2, 31.9, 30.7, 28.0. Anal.Calcd for C<sub>31</sub>H<sub>37</sub>N<sub>3</sub>O<sub>4</sub>Br<sub>2</sub>: C, 55.12; H, 5.52; N, 6.22. Found: C, 55.36; H, 5.77; N, 5.71. HRSMS (ES): [M+ H]<sup>+</sup> 674.1219 (calcd 674.1224)

#### Lem-PHEA

**Lem-In** (45 mg, 0.066 mmol), CuBr (26 mg, 0.135 mmol), and 2,2'-bipyridine (42 mg, 2.68 mmol) were dissolved in a mixture of THF (1mL) and HEA (1mL, 7.7 mmol). Argon was bubbled for 15 minutes, the tube was sealed, and the resulting reddish solution was stirred for 17 minutes at 85°C. Then, the solution was cooled rapidly by immersion in liquid nitrogen for 15 seconds, the tube was opened, its content was diluted in ca 10 mL of MilliQ water, put in a dialysis bag (MWCO = 1000 Da) and dialyzed against a large volume of MilliQ water (which was replaced at regular intervals) for 2 days. The resulting reddish solution was lyophilized yielding 120 mg of a fibrous solid.

<sup>1</sup>H NMR(CD<sub>3</sub>OD): δ(ppm) 7.5-6.75 (m, 7H), 4.13 (b, ≈40H), 3.73 (b, ≈40H), 2.38 (b, ≈20H), 1.75 (b, ≈40H) 1.10 (s, 6H), 1.04 (s, 12H). <sup>13</sup>C NMR (CD<sub>3</sub>OD): δ(ppm) 177.5, 175.3, 173.2, 169.2, 156.5, 149.5, 138.6, 129.7, 124.7, 124.5, 120.8, 113.9, 113.2, 111.3, 66.0, 62.0, 59.7, 53.5, 48.1, 42.6, 41.5, 38.7, 34.6, 31.6, 31.0, 27.6, 26.9. GPC Mn= 4737 Mw/Mn= 2.08

## Conclusions

We reported the synthesis and the spectroscopic study of a Lemke chromophore derivative bearing two water-solubilizing polymeric arms. We showed that the latter was soluble in water and physiological serum (0.5% aq. NaCl) above millimolar concentrations. The fluorescence is almost completely quenched, both for the polymeric object **Lem-PHEA** and its monomeric precursor **Lem-In** in low-polarity solvents, but strongly increases and is significantly red-shifted as solvents polarity is increased. The origin of this very unusual behaviour, *ie* a positive solvatochromism along with a negative solvatokinetic effect,

could be partly elucidated on the basis of theoretical calculations. It was shown by PCM-TD-DFT calculation that these effects were neither related to harmonic vibronic couplings nor to electrostatic interactions between the solute and the solvent, but most probably to an excited-state twisting of the terminal dicyano group. Although further studies are probably necessary to fully quantify the origin of the deviation from the energy gap law that we clearly evidenced in this work, this behaviour made it possible to obtain an efficient water soluble two-photon probe with absorption and polarity induced fluorescence in the NIR, with good quantum yield ( $\phi_f = 0.25 @ 676 \text{ nm}$ ) and two-photon cross section ( $\sigma_{\text{TPA}} = 440 \text{ GM} @ 1040 \text{ nm}$ ). Using TPLSM with this probe, we obtained three dimensional images of the functional cerebral vasculature in the motor cortex of mice, in a NIR-NIR (excitation-emission) configuration, with very high contrast and resolution. Meanwhile, we also showed that the probe was cleared by the renal system with no accumulation in the hepatic cells. This constitutes a very promising feature in the context of *in vivo* imaging, especially in view of diagnostic applications. We underline that, although Lemke chromophore derivatives had never been used previously, to the best of our knowledge, for biological imaging related applications *a fortiori in vivo*, the present contribution provides clear-cut evidences that this easily accessible class of molecules constitute valuable candidates for two-photon bio-imaging applications in the NIR.

## Acknowledgments

We thank Patrice L. Baldeck and J. Bernard for their precious help with two-photon induced fluorescence measurements (two-photon cross section determinations). We thank the *Région Rhône-Alpes* (Cluster 5) for PhD grant (JM) and fundings. A.C.E. thanks the European Research Council (ERC, Marches 278845) for his post-doctoral grant. D.J. acknowledges the European Research Council (ERC) and the *Région des Pays de la Loire* for financial support in the framework of a Starting Grant (Marches - 278845) and a *recrutement sur poste stratégique*, respectively. This research used resources of 1) the GENCI-CINES/IDRIS (Grant c2012085117), 2) CCIPL (*Centre de Calcul Intensif des Pays de Loire*), 3) a local Troy cluster. The intravital microscopy studies were performed on the France Life Imaging Platform at Grenoble.

## Notes and references

<sup>a</sup> *Laboratoire de Chimie, UMR CNRS-5182, Université de Lyon, Université Claude Bernard, École Normale Supérieure de Lyon, 46 allée d'Italie, 69364 Lyon, France Tel: (+33)472728860*

<sup>b</sup> *E-mail: xxxx@aaa.bbb.ccc*

<sup>c</sup> *CEISAM, UMR CNRS 6230, Université de Nantes, 2 rue de la Houssinière, 44322 Nantes cedex 3, France. Fax: 33251125712; Tel: 33251125564*

<sup>d</sup> *Grenoble Institute of Neuroscience (GIN), Inserm U 836 – Université Joseph Fourier - CEA – CHU, Chemin Fortuné Ferrini, 38042, La Tronche Cedex*

<sup>e</sup> *Institut Universitaire de France, 103, bd Saint-Michel, F-75005 Paris Cedex 05, France*

<sup>†</sup> Electronic Supplementary Information (ESI) available: Polarity plot and calculation of the ground and excited state dipole moments. Plot of the emission lifetime and of radiative and nonradiative kinetic constants for the excited state decay vs emission energy. <sup>1</sup>H and <sup>13</sup>C NMR for **Lem-OH**, **Lem-In** and **Lem-PHEA**. Computed bond lengths for a model molecule (**Lem**) at its ground and excited states. Dependence on the

ground and excited state energy on choosen angular deformations within the molecule. GPC characterization of Lem-PHEA. Overlay of the emission of Lem-PHEA in water and the detector's ranges in Red and NIR configurations, and comparisons of the respective signal intensities in red and NIR configuration. Pictures evidencing renal clearance of teh dye, and its absence of accumulation in hepatic cells See DOI: 10.1039/b000000x/

1. H. Kobayashi, M. Ogawa, R. Alford, P. L. Choyke and Y. Urano, *Chem. Rev.*, 2009, **110**, 2620-2640.
2. F. Leblond, S. C. Davis, P. A. Valdés and B. W. Pogue, *J. Photochem. Photobiol. B*, 2010, **98**, 77-94.
3. J. Rao, A. Dragulescu-Andrasi and H. Yao, *Curr. Opin. Biotechnol.*, 2007, **18**, 17-25.
4. T. Terai and T. Nagano, *Curr. Opin. Biotechnol.*, 2008, **12**, 515-521.
5. C. Reichardt, *Chem. Rev.*, 1994, **94**, 2319-2358.
6. M. Albota, D. Beljonne, J.-L. Brédas, J. E. Ehrlich, J.-Y. Fu, A. A. Heikal, S. E. Hess, T. Kogej, M. D. Levin, S. R. Marder, D. McCord-Maughon, J. W. Perry, H. Röckel, M. Rumi, G. Subramaniam, W. W. Webb, X.-L. Wu and C. Xu, *Science*, 1998, **281**, 1653-1656.
7. J. L. Bredas, C. Adant, P. Tackx, A. Persoons and B. M. Pierce, *Chem. Rev.*, 1994, **94**, 243-278.
8. G. S. He, L.-S. Tan, Q. Zheng and P. N. Prasad, *Chem. Rev.*, 2008, **108**, 1245-1330.
9. D. R. Kanis, M. A. Ratner and T. J. Marks, *Chem. Rev.*, 1994, **94**, 195-242.
10. D. Cui, X. Qian, F. Liu and R. Zhang, *Org. Lett.*, 2004, **6**, 2757-2760.
11. M.-H. Zheng, J.-Y. Jin, W. Sun and C.-H. Yan, *New J. Chem.*, 2006, **30**, 1192-1196.
12. M. Y. Berezin, H. Lee, W. Akers and S. Achilefu, *Biophys. J.*, 2007, **93**, 2892-2899.
13. R. W. Sinkeldam and Y. Tor, *Org. Biomol. Chem.*, 2007, **5**, 2523-2528.
14. H. Cao and M. D. Heagy, *J. Fluoresc.*, 2004, **14**, 569-584.
15. Z. Xu, X. Qian and J. Cui, *Org. Lett.*, 2005, **7**, 3029-3032.
16. M. Yin, K. Ding, R. A. Gropeanu, J. Shen, R. d. Berger, T. Weil and K. Mullen, *Biomacromolecules*, 2008, **9**, 3231-3238.
17. M. Yin, J. Shen, R. Gropeanu, G. O. Pflugfelder, T. Weil and K. Müllen, *Small*, 2008, **4**, 894-898.
18. M. Yin, J. Shen, G. O. Pflugfelder and K. Mullen, *J. Am. Chem Soc.*, 2008, **130**, 7806-7807.
19. C. Monneréau, S. Marotte, P.-H. Lanoe, O. Maury, P. Baldeck, D. Kreher, A. Favier, M.-T. Charreyre, J. Marvel, Y. Leverrier and C. Andraud, *New J. Chem.*, 2012, **36**, 2328-2333.
20. W. Denk, J. Strickler and W. Webb, *Science*, 1990, **248**, 73-76.
21. F. Helmchen and W. Denk, *Nat. Methods*, 2005, **2**, 932-940.
22. S. A. Hilderbrand and R. Weissleder, *Curr. Opin. Biotechnol.*, 2010, **14**, 71-79.
23. V. Chynwat and H. A. Frank, *Chem. Phys.*, 1995, **194**, 237-244.
24. R. Englman and J. Jortner, *Mol. Phys.*, 1970, **18**, 145-164.
25. J. V. Caspar, E. M. Kober, B. P. Sullivan and T. J. Meyer, *J. Am. Chem Soc.*, 1982, **104**, 630-632.
26. A. L. Macanita, F. P. Costa, S. M. B. Costa, E. C. Melo and H. Santos, *J. Phys. Chem.*, 1989, **93**, 336-343.
27. M. H. Gehlen and F. C. De Schryver, *Chem. Rev.*, 1993, **93**, 199-221.
28. R. Lemke, *Synthesis*, 1974, **1974**, 359-361.
29. J. Massin, W. Dayoub, J.-C. Mulatier, C. Aronica, Y. Bretonnière and C. Andraud, *Chem. Mater.*, 2010, **23**, 862-873.
30. D. R. Larson, W. R. Zipfel, R. M. Williams, S. W. Clark, M. P. Bruchez, F. W. Wise and W. W. Webb, *Science*, 2003, **300**, 1434-1436.
31. M. J. Levene, D. A. Dombeck, K. A. Kasischke, R. P. Molloy and W. W. Webb, *J. Neurophys.*, 2004, **91**, 1908-1912.
32. S. Ermer, S. M. Lovejoy, D. S. Leung, H. Warren, C. R. Moylan and R. J. Twieg, *Chem. Mater.*, 1997, **9**, 1437-1442.
33. R. Andreu, S. Franco, E. Galán, J. Garín, N. Martínez de Baroja, C. Momblona, J. Orduna, R. Alicante and B. Villacampa, *Tetrahedron Lett.*, 2010, **51**, 3662-3665.
34. L. Chen, G. Qian, Y. Cui, X. Jin, Z. Wang and M. Wang, *J. Phys. Chem. B*, 2006, **110**, 19176-19182.
35. I. Rau, P. Armatys, P. A. Chollet, F. Kajzar, Y. Bretonnière and C. Andraud, *Chem. Phys. Lett.*, 2007, **442**, 329-333.

- 
36. Q. Zhang, Y. Tu, H. Tian and H. Ågren, *J. Phys. Chem. B*, 2007, **111**, 10645-10650.
37. J. Li, D. Liu, Z. Hong, S. Tong, P. Wang, C. Ma, O. Lengyel, C.-S. Lee, H.-L. Kwong and S. Lee, *Chem. Mater.*, 2003, **15**, 1486-1490.
- 5 38. L. Yang, M. Guan, D. Nie, B. Lou, Z. Liu, Z. Bian, J. Bian and C. Huang, *Opt. Mater.*, 2007, **29**, 1672-1679.
39. G. Weber and F. J. Farris, *Biochemistry*, 1979, **18**, 3075-3078.
40. E. G. McRae, *J. Phys. Chem.*, 1957, **61**, 562-572.
41. E. Lippert, *Ber. Bunsen Ges. Phys. Chem.*, 1957, **61**, 962-975.
- 10 42. P. Suppan, *J. Photochem. Photobiol. A*, 1990, **50**, 293-330.
43. N. Mataga, Y. Kaifu and M. Koizumi, *Bull. Chem. Soc. Jpn*, 1956, **29**, 465-470.
44. Q. Peng, Y. Yi, Z. Shuai and J. Shao, *J. Am. Chem Soc.*, 2007, **129**, 9333-9339.
- 15 45. R. F. Goldstein and W. Bialek, *Phys. Rev. B*, 1983, **27**, 7431-7439.
46. although CI intersection between two states cannot be fully optimized with a LR-TD-DFT scheme the characteristic evolution of the GS and ES potential curves near 90° twist angle constitutes good support to our hypothesis. Of course, CAS or MR approaches that allow CI optimization are both out of reach for a dye presenting a such a large conjugated backbone
- 20 47. M. Fox, E., F. Szoka and J. M. J. J. Fréchet, *Acc. Chem. Res.*, 2009, **42**, 1141-1151.
48. C. Xu and W. W. Webb, *J. Opt. Soc. Am. B*, 1996, **13**, 481-491.
- 25 49. D. Jacquemin, A. Planchat, C. Adamo and B. Mennucci, *J. Chem. Theory Comput.*, 2012, **8**, 2359-2372.
50. F. Santoro, R. Improta, A. Lami, J. Bloino and V. Barone, *J. Chem. Phys.*, 2007, **126**, 084509-084513.
51. F. Santoro, A. Lami, R. Improta and V. Barone, *J. Chem. Phys.*, 2007, **126**, 184102-184111.
- 30 52. J. Tomasi, B. Mennucci and R. Cammi, *Chem. Rev.*, 2005, **105**, 2999-3094.
53. R. Improta, V. Barone, G. Scalmani and M. J. Frisch, *J. Chem. Phys.*, 2006, **125**, 054103-054109.
- 35 54. Frisch, M. J.; Trucks, G. W.; Schlegel, H. B.; Scuseria, G. E.; Robb, M. A.; Cheeseman, J. R.; Scalmani, G.; Barone, V.; Mennucci, B.; Petersson, G. A.; Nakatsuji, H.; Caricato, M.; Li, X.; Hratchian, H. P.; Izmaylov, A. F.; Bloino, J.; Zheng, G.; Sonnenberg, J. L.; Hada, M.; Ehara, M.; Toyota, K.; Fukuda, R.; Hasegawa, J.; Ishida, M.; Nakajima, T.; Honda, Y.; Kitao, O.; Nakai, H.; Vreven, T.; Montgomery, J. A., Jr.; Peralta, J. E.; Ogliaro, F.; Bearpark, M.; Heyd, J. J.; Brothers, E.; Kudin, K. N.; Staroverov, V. N.; Kobayashi, R.; Normand, J.; Raghavachari, K.; Rendell, A.; Burant, J. C.; Iyengar, S. S.; Tomasi, J.; Cossi, M.; Rega, N.; Millam, J. M.; Klene, M.; Knox, J. E.; Cross, J. B.; Bakken, V.; Adamo, C.; Jaramillo, J.; Gomperts, R.; Stratmann, R. E.; Yazyev, O.; Austin, A. J.; Cammi, R.; Pomelli, C.; Ochterski, J. W.; Martin, R. L.; Morokuma, K.; Zakrzewski, V. G.; Voth, G. A.; Salvador, P.; Dannenberg, J. J.; Dapprich, S.; Daniels, A. D.; Farkas, O.; Foresman, J. B.; Ortiz, J. V.; Cioslowski, J.; Fox, D. J. *Gaussian 09, Revision A.02*; Gaussian Inc.: Wallingford, CT, 2009.
- 40 45 50 55 56. D. Jacquemin, T. L. Bahers, C. Adamo and I. Ciofini, *Phys. Chem. Chem. Phys.*, 2012, **14**, 5383-5388.
57. W. S. Rasband, <http://rsb.info.nih.gov/ij/>, 1997-2011.